J. Fluid Mech. (1983), *vol.* 128, *pp.* 413–426
Printed in Great Britain

The velocity perturbations above the orifice of an acoustically excited cavity in grazing flow

By A. F. CHARWAT AND B. E. WALKER
Department of Mechanics and Structures, School of Engineering and Applied Science, University of California, Los Angeles, CA 90024

(Received 23 February 1982 and in revised form 5 October 1982)

Detailed measurements of the time-dependent velocities induced inside and outside the opening of an acoustically excited, two-dimensional Helmholtz resonator imbedded in a grazing flow are presented. The remarkably clear structure of the perturbation field which evokes a pulsating source and a coherently pulsating vortex-image pair is described.

1. Introduction

Helmholtz resonators, which are cavities coupled to the environment through a constricting orifice, exhibit a marked increase in acoustic resistance and a decrease in reactance, the real and imaginary parts of the acoustic impedance respectively, when there is grazing flow over the orifice. The acoustic impedance is the ratio of the external harmonic pressure perturbation impinging on the resonator to the cyclical volume velocity (flow rate per unit area) into the cavity.

The acoustic phenomena are well documented experimentally for a variety of configurations of the orifice, intensities of the excitation and velocities of the grazing flow (see e.g. Hersh & Walker 1979; Kopenhans & Ronneberger 1980). The resistance varies slowly at first, and, at a grazing velocity which seems to depend on the Strouhal number based on the characteristic dimension of the orifice, begins to increase linearly with the grazing velocity: its slope is not sensitive to the frequency and the level of the excitation. Rice (1976), Rogers & Hersh (1976) and Hersh & Walker (1979) formulated models which ultimately tie this phenomenon to a discharge coefficient of the orifice. These models portray the behaviour of the acoustic resistance well; however, the observed changes in the inertance of the resonator elude satisfactory explanation.

There are only a few studies of the actual flow field in and immediately above the orifice. Baumeister & Rice (1976) used a water channel and dye visualization to observe it. The cyclical flow into the cavity was pumped artifically; the experiment does not fully represent the actual problem but its general features are much like those we describe in what follows. Ingard & Labate (1950) and Ingard & Ising (1967) studied an acoustically excited resonator, but the cavity discharged into a stationary atmosphere. They demonstrated that the cycle is asymmetrical: the inflow is essentially potential while the outflow leads to the formation of a distinct free jet out of the orifice.

The objective of the present experiments is to map out the unsteady near field around the orifice of a resonator discharging into a tangential flow. The level of the external excitation is sufficiently high to override the self-generated oscillations of the separated shear layer. The wavelength of the external perturbation is much larger

than the characteristic dimension of the orifice (the excitation frequency is 100 Hz). In order to facilitate the interpretation of the structure of the perturbation field, a two-dimensional orifice is used, i.e. the cavity is coupled to the flow through a high-aspect-ratio slot. Measurements of the pressure variation in the cavity and on the orifice plate, which constitute the standard 'two-microphone' method of determining the acoustic impedance of resonators, showed that the two-dimensionality of the configuration does not change the character of the variation of the impedance, except that the slope of the resistance–velocity curve is larger by a factor of about two compared with resonators with circular orifices.

A large amount of data is involved, of which only examples illustrating the structure of the flow field are given in this paper. The two cases quoted fall respectively in the fully developed high-speed regime of linearly varying acoustic resistance and in the transition regime at the knee of the resistance curve. A more complete compilation of results is available in Walker (1981) and Charwat & Walker (1981).

2. Description of the experiment

The wind-tunnel model consisted of a rectangular cavity coupled to the flow in the test section through a high-aspect-ratio slot 7·62 mm wide (in the streamwise direction) and 155 mm long (normal to the flow). The thickness of the slot was 6·35 mm. (The slot is shown to scale on figures 3, 5 and 6; the grazing flow is from right to left). The volume of the cavity was 0·0133 m^3, which tuned the resonator to 100 Hz (no grazing flow). Excitation was provided by a 200 W speaker mounted in the roof of the tunnel, directly (0·8 m) above the slot. The experiments were conducted at a constant frequency (100 Hz) and a constant sound pressure level of 120 dB (re 20 μPa). Four grazing-flow velocities in the range 7·6–30 m/s were tested. Suction through a strip of porous wall upstream of the slot was used to thin out the boundary layer; its momentum thickness varied from 10–15 % of the width of the slot. The acoustic velocity perturbation was uniform along the span of the slot to within one slot width from the edges, and the incident pressure measured at the orifice, orifice closed, was not vitiated by reflections involving the tunnel.

Pressures were measured in the resonator cavity and on the orifice plate with flush-mounted microphones; each instrument and its individual pre-amplifier were calibrated for attenuation and phase shift against a common reference. The velocities were measured using a Thermal Systems Inc. split-film anemometer, which, because of its central role, will be described in additional detail below. The anemometer could survey an area of about 5×5 cm in the plane normal to the slot with a resolution of 0·127 mm. The minimum distance of approach to the wall (measured from the centerline of the probe) was 0·3 mm, 4 % of the slot dimension.

The TSI 'split-film' probe is a directional hot-film anemometer which consists of two separate sensors deposited each on approximately half of the circumference of a quartz fibre, 0·15 mm in diameter. The sum of the heating currents supplied to both films is proportional to the quarter-power of the mean velocity as in ordinary hot-wire anemometry; the difference of the squared currents is approximately proportional to the sine of the angle of the flow relative to the plane of the 'split'. Two such probes placed side by side with split planes at 90° to each other were used to identify the velocity components in four quadrants.

The calibration of the split-film probe is not as simple as that of a single-element hot wire. This arises from the thermal coupling of the half-films by conduction

through their common substrate. Instead of using an analytical approximation to its behaviour, the probe outputs were reduced by direct comparison with calibration data stored in the memory of a microprocessor. The look-up table contained 8192 entries in steps of 1·8° in the orientation of the probe over $\pm 90°$ and logarithmically distributed velocity intervals in the range 0·12–38 m/s. The calibration procedure was carried out using exactly the same signal-acquisition chain as that used to collect data, ensuring that nonlinearities in the electronic components were accounted for.

The transient response of the instrument is a function of its orientation, the mean velocity and the frequency of the disturbance, as well as the overheat ratio and bridge balance (see Ho 1982). While it appears possible to reconstitute the true input waveform by a linearized iterative procedure, this is not practical. A single phase shift and attenuation correction corresponding to the mean operating condition was used in the present reduction procedure. The resulting uncertainty in the phase information is estimated at 5° and that in the amplitudes at 3%.

Velocity gradients over a distance of the order of the diameter of the probe can be expected to result in a false indication of its orientation of the flow. To gain some insight into this problem, the probe was used to traverse the wake immediately downstream of a 4 cm symmetrical airfoil at several stations 0·25 mm apart. The measured streamwise velocity and two-dimensional continuity were used to calculate the cross-velocity. This was compared to the cross-velocity indicated by the probe. At the station closest to the trailing edge (0·51 mm downstream of it) the maximum divergence between the two results amounted to about 15%. The velocity gradient at this station is about 10^4 inverse seconds, comparable to the highest shear encountered above the test orifice. The internal consistency of this test is clearly encouraging; at stations further downstream progressively better accord was obtained.

The entire data-acquisition procedure was controlled by the microprocessor. It generated the acoustic excitation as a 64-segment approximation to a harmonic function. The data were sampled at each of the 64 phase intervals over 4000 cycles, sorted, averaged, reduced and stored on magnetic disks in real time. Cavity and tunnel reference pressures were acquired once every 5 cycles. After completing the measurements at 75 positions the probe was automatically returned to a free-stream reference location for recalibration against drift. A survey of the flow over the orifice at one grazing velocity required 15 h of continuous testing.

An overall evaluation of the accuracy of the present results is obtained by integrating the normal velocity component into the orifice for a full cycle. If the angle of the free stream at the reference station (one orifice length upstream and two lengths above the wall) is set to zero, we find a small mean inward flux into the wall; alternatively, if the net inflow is set to zero, the flow at the reference station is found to diverge from the wall by 3–6°. This can be partly explained by a displacement effect of the boundary layer.

3. Results

The direct measurements consist of waveforms of the velocity components. Figure 1 shows an example of their development with distance from the wall at a station 25% from the leading edge of the slot and at the downstream edge. Velocities are referenced to the maximum nominal volume velocity calculated from the derivative of the fluctuations of the pressure in the cavity. The streamwise velocity is plotted relative to its local average.

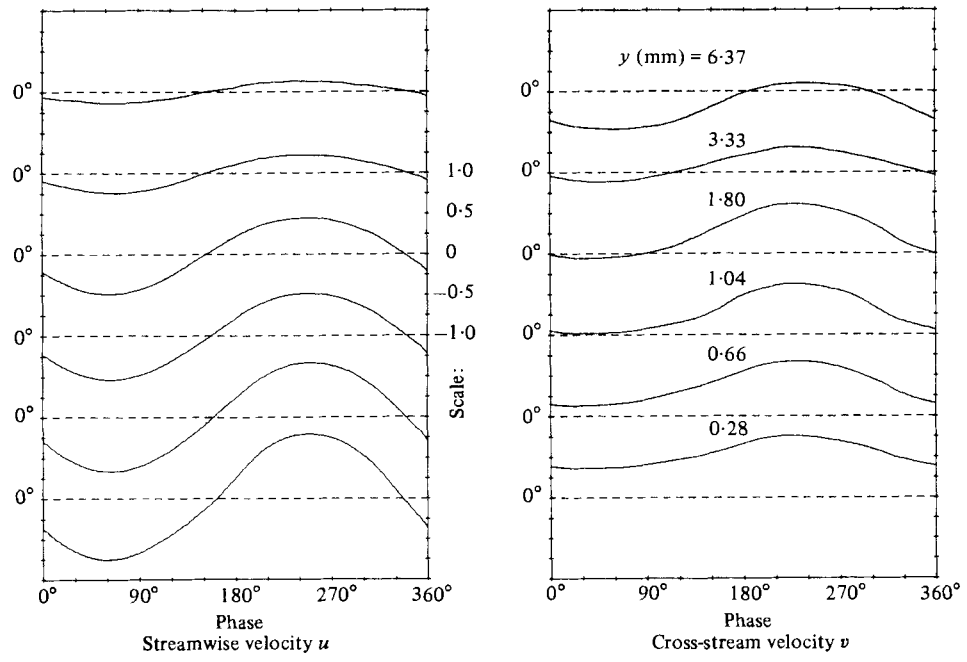

(*a*)

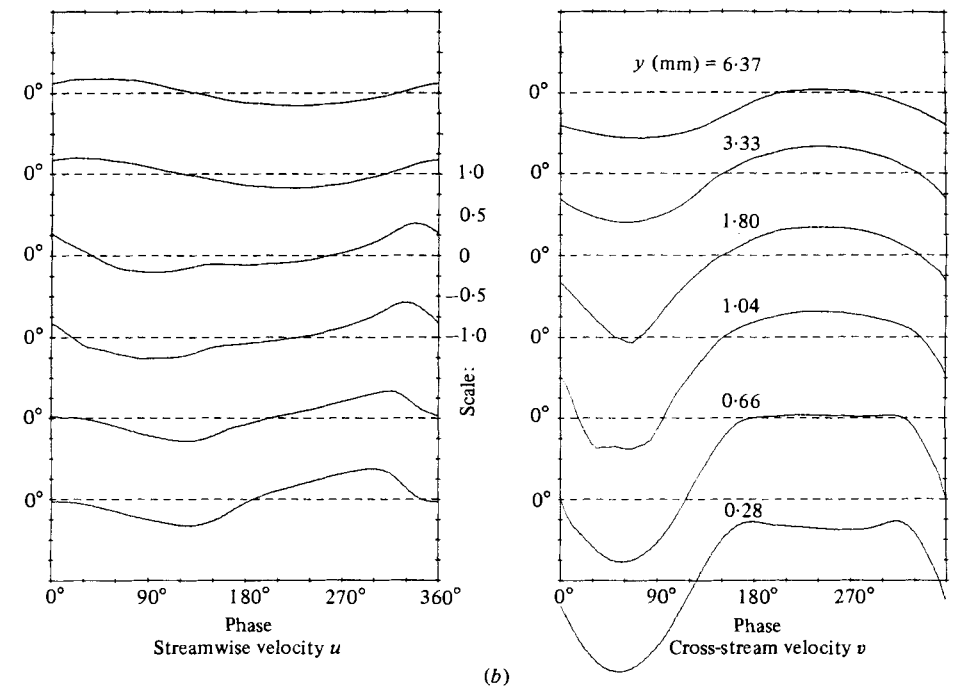

(*b*)

FIGURE 1. Waveforms of the perturbation velocities: (*a*) at 25 % of the slot width from separation; (*b*) above the downstream corner of the slot. Various distances (y) from the wall. Grazing velocity: 22·9 m/s.

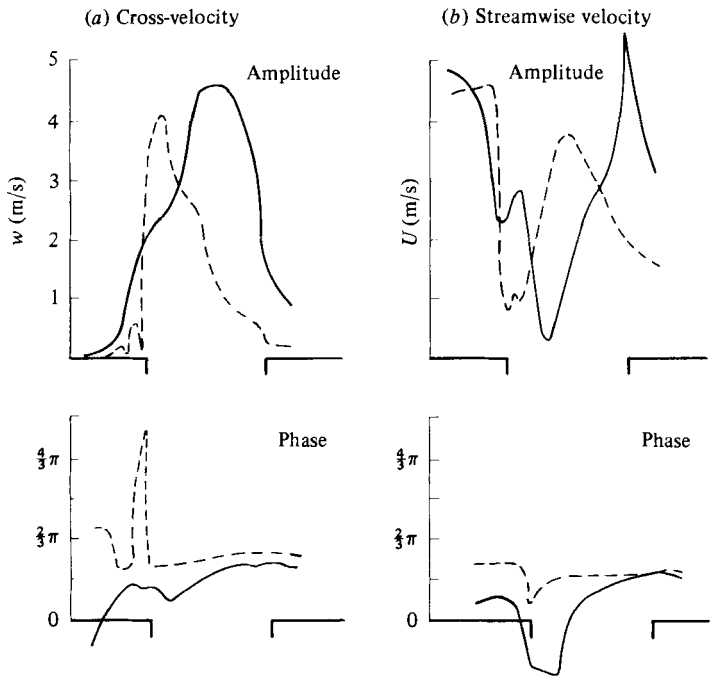

FIGURE 2. Streamwise variation of the amplitudes and phase, first harmonic of the velocities, 4% of the slot width above the wall. – – – –, 28·9 m/s; ——, 7·6 m/s.

It is difficult to interpret the raw results. The distortion of the individual waveforms increases towards the wall and the downstream corner of the orifice. In spite of this, the waveform of the space-averaged cross-velocity over the plane immediately above the orifice, i.e. the variation of the volume flow into the orifice, is remarkably sinusoidal. This checks the relatively pure harmonic variation of the pressure in the cavity, examples of which are shown on figure 4. A general characteristic of the waves, particularly noticeable at higher grazing velocities, is that the inflow phase seems to last somewhat longer than half the cycle while the outflow is compressed in time. The largest perturbations occur near the downstream corner of the orifice. Note the phase reversal in the streamwise velocity at about 2 mm from the wall on figure 1 (*b*) (this does not happen at low grazing speeds).

Typical plots of the phase and amplitude of the first harmonic of the waves along the wall are shown on figure 2. For a simple line source the streamwise and normal velocity are antisymmetrical and bell-shaped, respectively. The phase of the former changes discontinuously by π at the centreline and that of the latter is constant. In a general sense these features are present in figure 2. As the grazing velocity increases, the axis of the perturbation field is swept downstream. Also, its spread is decreased. It appears as if only the downstream portion of the orifice remained 'open' at higher grazing velocities.

The magnitude of the perturbations decreases with grazing velocity. Pronounced irregularities appear immediately downstream of the attachment corner, indicating local separation and flow reversal. (Note that at low grazing velocities we also observe local separation of the upstream wall during the outflow half-cycle – see Walker & Charwat (1982).) The curves show local peaks; their evolution from one station to another can be followed with remarkable consistency on a complete set of these

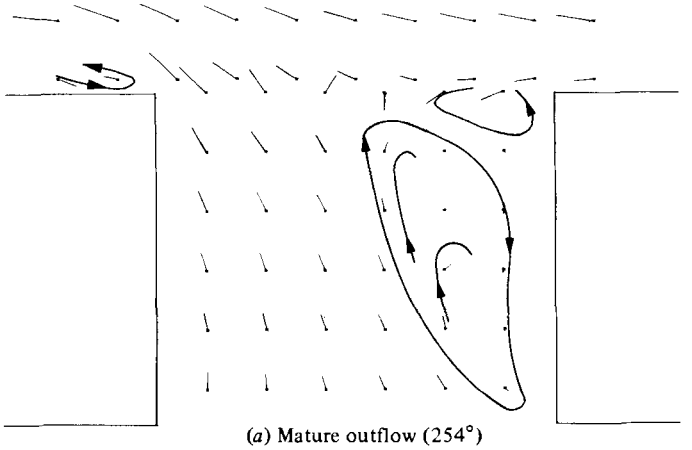

(*a*) Mature outflow (254°)

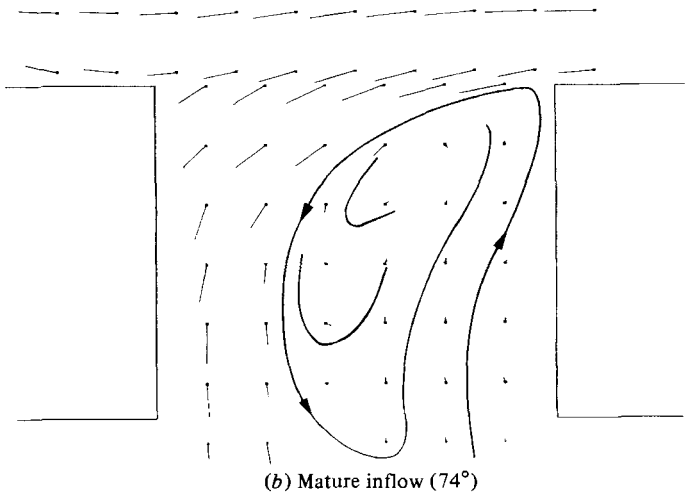

(*b*) Mature inflow (74°)

FIGURE 3. Flow patterns in the slot. Grazing velocity: 15 m/s from right to left.

results. The distorted near field extends from the order of one half (at high speed) to one slot width into the flow.

The channelling of the flow into the slot is evident from the patterns shown in figure 3. These are measurements inside the passage at the grazing velocity of 15 m/s (unfortunately a complete set of data inside the passage was not obtained because of damage to our probe). We selected the two phase-points depicting most clearly the 'mature' inflow and outflow patterns (which are emphasized by freehand traces). Note that these phase points are offset relative to the phase of the volume velocity. Each pattern 'unravels' during transition from inflow to outflow.

The variation of the pressure on the sides of the slot 1 mm below the corner is shown in figure 4. The cavity pressure is also plotted as a reference. With no grazing flow, the pressure is instantaneously uniform across the orifice and its variation in time is approximately symmetrical with respect to that of the pressure in the cavity. Local minima occur at about the zero-crossings of the cavity pressure: these correspond to a maximum velocity through the orifice and thus appear to be associated with the dynamic pressure drop in the flow through the orifice. With grazing flow, the pressure

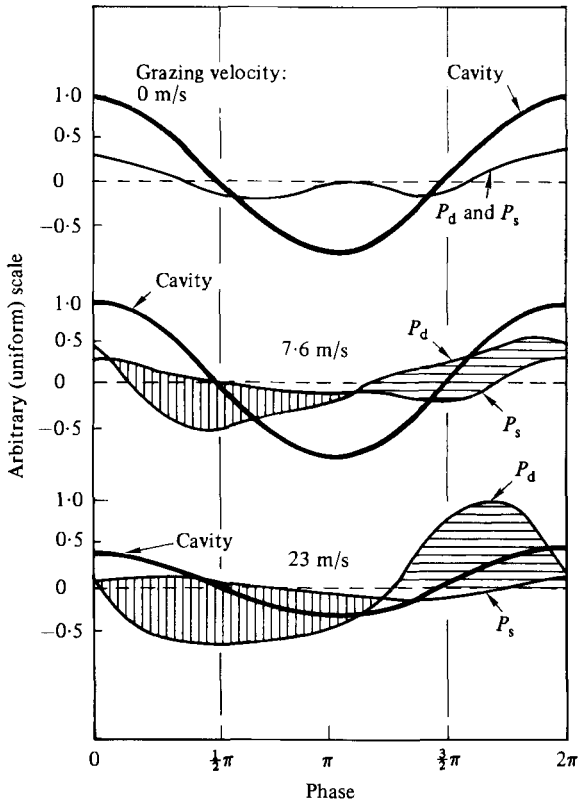

FIGURE 4. Variation of the pressure on the side of the slot 1 mm below the corners; P_d, downstream face; P_s, upstream face.

on the downstream face increases relative to that on the upstream face during inflow and falls below it during outflow. These observations indicate respectively a significant recovery of dynamic pressure of the external flow and sharp centrifugal gradients associated with the turning of the exhaust jet around the downstream corner. The peak gradients lag the cavity pressure by about 30°, i.e. the maximum velocity in the opening is no longer in phase with the average velocity (volume flow) into the cavity.

Perhaps the clearest picture emerges from a sequence of maps of instaneous vector velocity perturbations (relative to the local mean). This is shown on figures 5 (*a–d*) in sufficient detail to demonstrate the evolution of the flow at a grazing velocity of 22·9 m/s. Figure 6 shows the same results for the low-grazing-velocity case (7·6 m/s) in larger time steps. The phase relative to the effective volume velocity (rate of change of the pressure in the cavity) is indicated in the right-hand corner of each picture.

The pattern of this unsteady local perturbation field implies a pulsating source and a coherently pulsating vortex pair downstream of the source, with the wall as the plane of symmetry. The stream function representing such a flow can be easily written down. The data indicates the location of the vortex is essentially fixed, at least to first order. This supplies a geometrical scale (conceptually, the width of the slot) and a condition relating the strengths of the source and the vortex. The resulting description involves two parameters: the source strength and the minimum separation of the vortex pair (distance of closest approach of the external vortex to the wall).

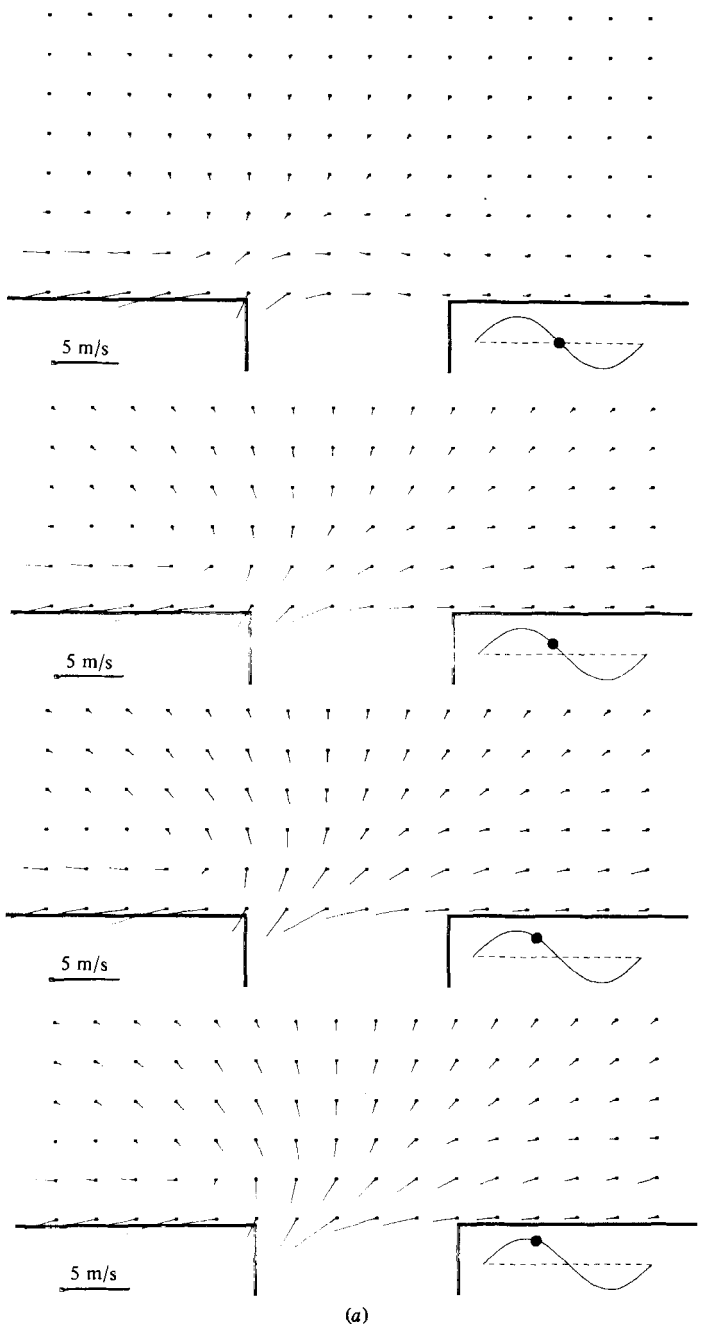

(*a*)

FIGURE 5(*a*). For caption see p. 423.

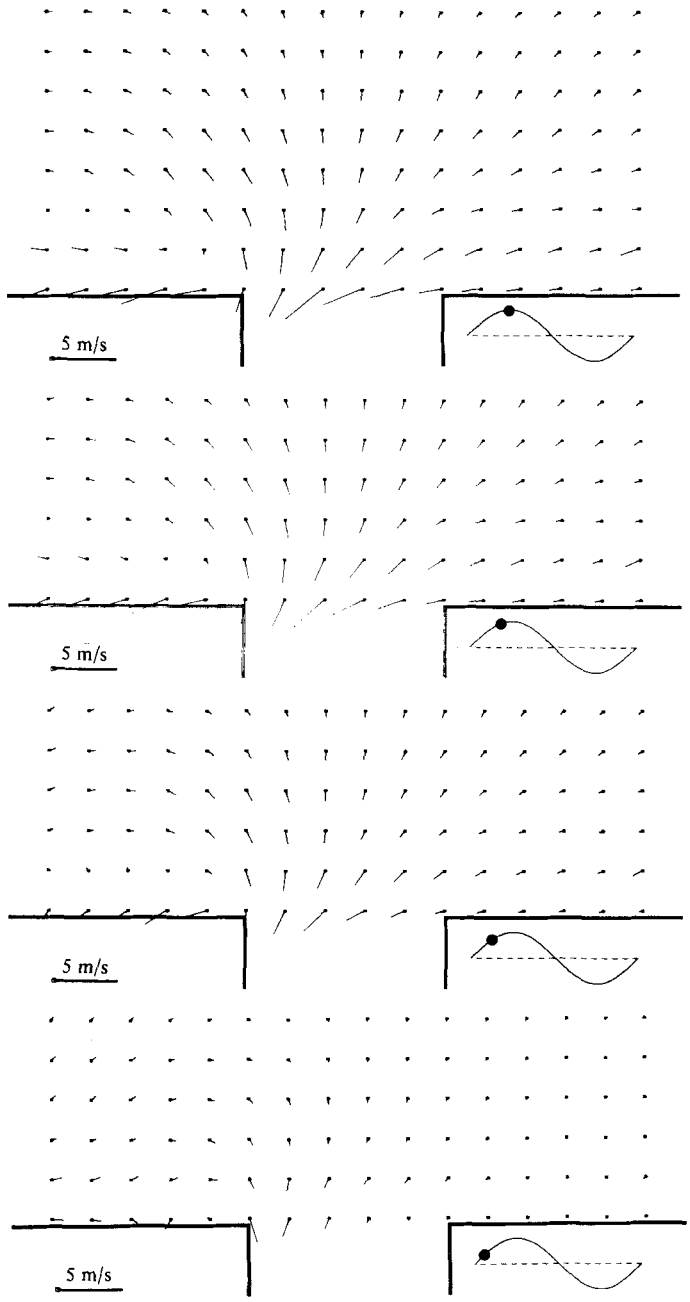

(*b*)

FIGURE 5(*b*). For caption see p. 423.

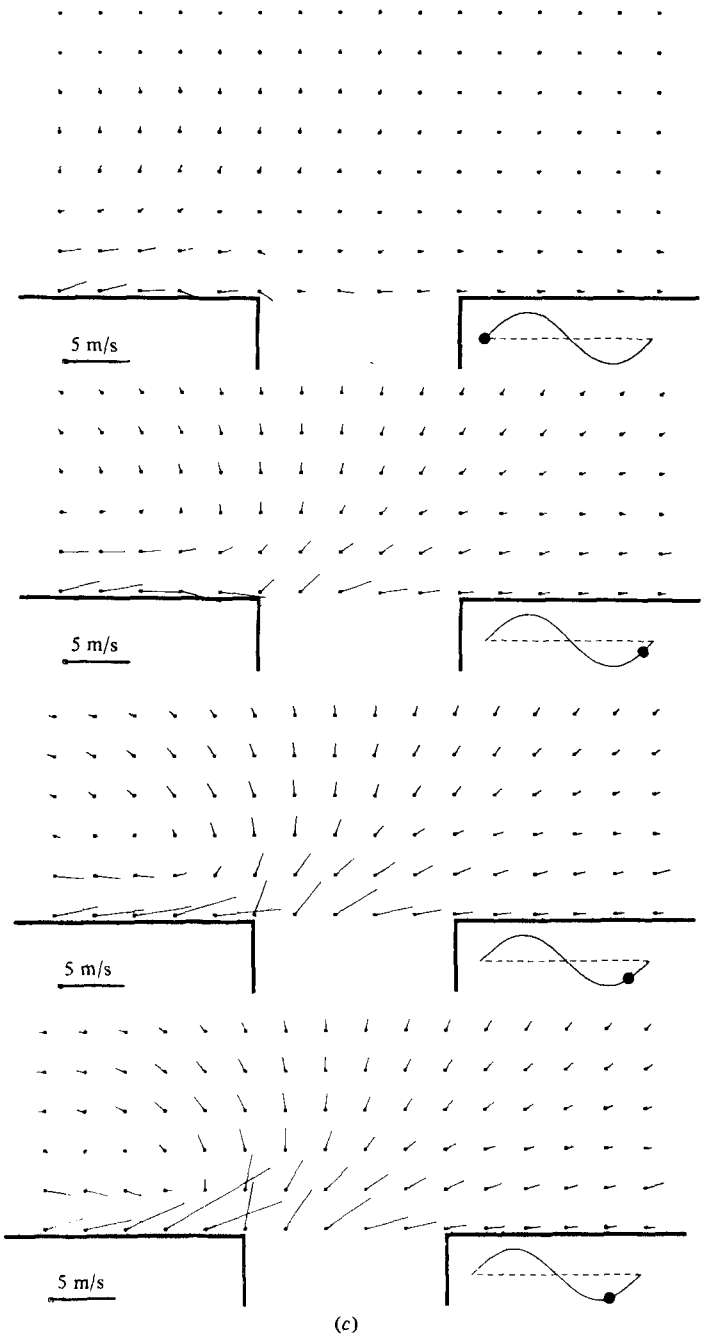

(c)

FIGURE 5(c). For caption see facing page.

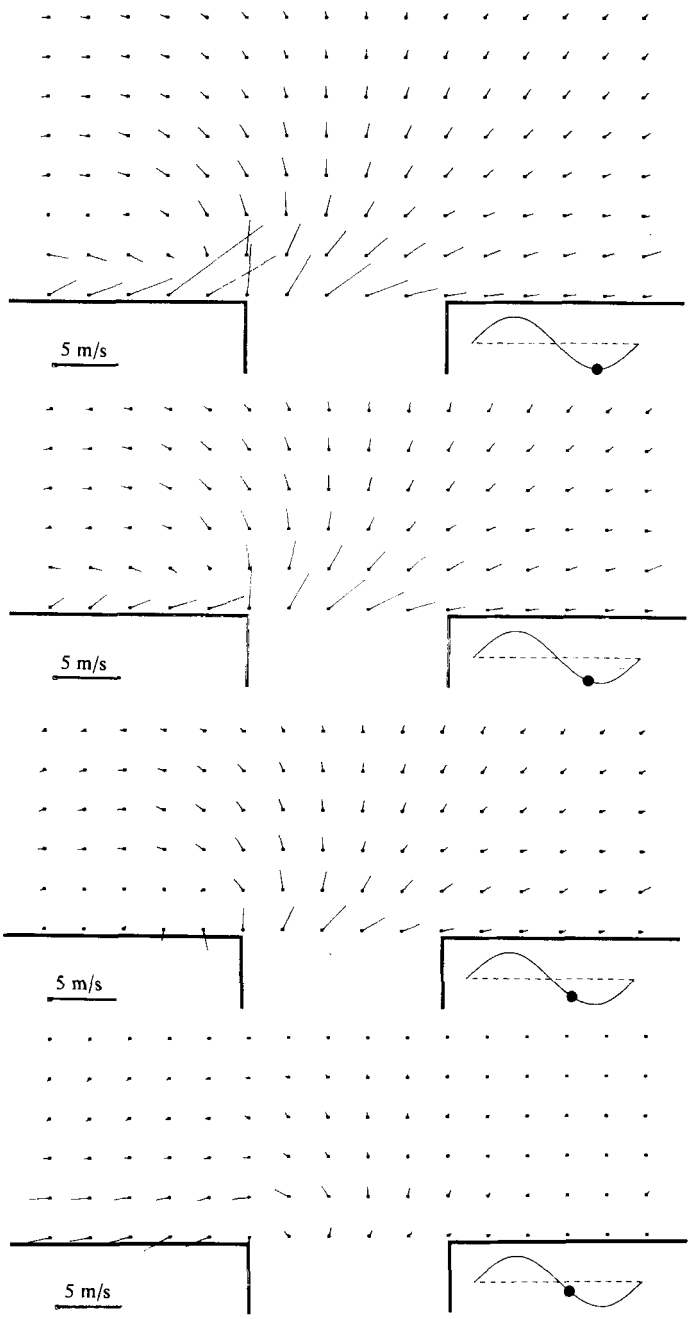

(*d*)

FIGURE 5. Evolution of the vector perturbation field above the slot (phase relative to volume flow indicated). Grazing velocity: 22·9 m/s from right to left.

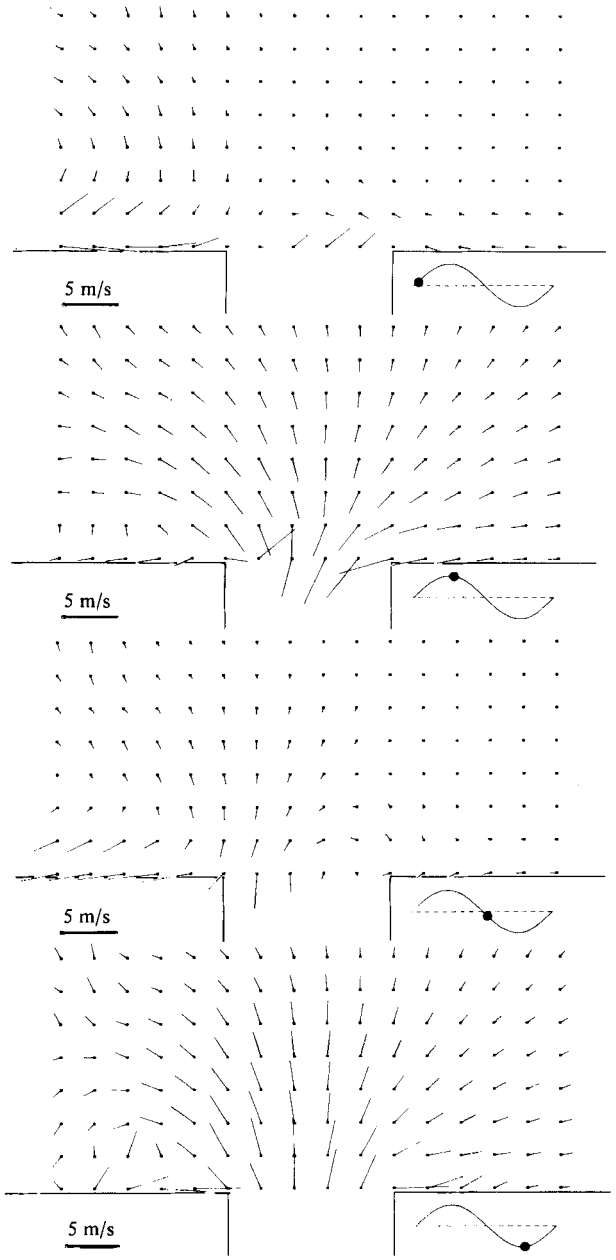

FIGURE 6. Evolution of the vector perturbation field above the slot (phase relative to volume flow indicated). Grazing velocity: 7·6 m/s from right to left.

Plots of such a stream function reproduce the measured structure of the flow field remarkably well thoughout the cycle (for the time being the two parameters of the problem must be assigned arbitrarily).

The advantage of the representation in terms of local unsteady perturbations is that it yields a comprehensible picture. Figure 7 complements this picture by showing the time-averaged perturbation vectors for test conditions corresponding to figure 5, referenced here to the profile of the upstream boundary layer. The latter is also

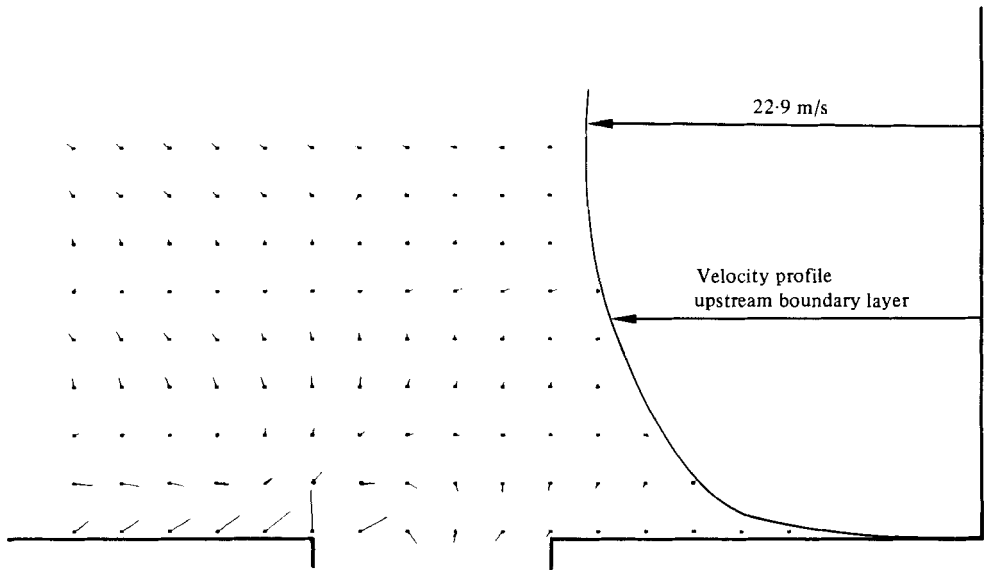

FIGURE 7. Steady component of the local perturbation field relative to the boundary-layer profile. Grazing velocity: 22·9 m/s.

shown on figure 7. The instantaneous total (true) velocity at any point is the sum of the unsteady local-perturbation vector (figure 5), the steady component of the perturbation vector and the boundary-layer velocity (figure 7) at the height under consideration above the wall.

Figure 7 shows a weak inward flow into the upstream two-thirds of the slot and outflow across the downstream one-third of it; the orifice appears to contain a steady vortex which rotates in the sense opposite to that of the vorticity in the oncoming boundary layer. Associated with it, one finds a counter-rotating vortex in the external near field downstream of reattachment. The apparent plane of symmetry of this vortex pair is at an angle of attack to the flow. It appears to be an interesting example of 'acoustic streaming'. At lower grazing velocities one obtains the same structure, less well defined and seemingly symmetrical about a plane more nearly parallel to the wall.

4. Conclusion

The objective of this experiment was to provide a description of the interaction between a grazing flow and the acoustically induced velocity perturbations in the neighbourhood of the orifice of a Helmholtz resonator. It was successful in that it yielded not only a base of quantitative data but also in that it suggested a definite structure of the perturbation field which can hopefully lend itself to analytical modelling.

This research was supported by a grant from NASA Lewis Research Center; we are particularly grateful for the encouragement and sustained support received from Dr E. Rice, Head, Noise Abatement Section, who monitored this project.

REFERENCES

BAUMEISTER, K. J. & RICE, E. J. 1976 Visual study of the effect of grazing flow on the oscillatory flow in a resonator orifice. *NASA TM* X-3288.

CHARWAT, A. F. & WALKER, B. E. 1981 The velocity field near the orifice of a Helmholtz resonator in grazing flow. *University of California at Los Angeles Rep.* ENG-81-101.

CHIH-MING HO 1982 *Rev. Sci. Instrum.* **53**, 1240.

HERSH, A. S. & WALKER, B. E. 1979 Effect of grazing flow on the acoustic impedance of Helmholtz resonators consisting of single and clustered orifices. *NASA* CR-3177.

INGARD, K. V. & ISING, H. 1967 *J. Am. Soc. Acoustics* **42**, 921.

INGARD, K. V. & LABATE, S. 1950 *J. Am. Soc. Acoustics* **22**, 211.

KOPENHANS, J. & RONNEBERG, D. 1980 The acoustic impedance of orifices in the wall of a flow duct with a laminar or turbulent flow boundary layer. *Am. Inst Aero. & Astro. 6th Aeroacoustic Conf., Paper* 80-0990.

RICE, E. J. 1976 A theoretical study of the acoustic impedance of orifices in the presence of a steady grazing flow. *NASA TM* X-71903.

ROGERS, T. & HERSH, A. S. 1976 Effect of grazing flow on steady-state resistance of isolated square edged orifices. *NASA* CR-2681.

WALKER, B. E. 1981 The relationship between the acoustic impedance and unsteady flow field near the orifice of a two-dimensional Helmholtz resonator. Ph.D. dissertation, School of Engineering, University of California.

WALKER, B. E. & CHARWAT, A. F. 1982 *J. Acoust. Soc. Am.* **72**, 550.